Inorganic Chemistry

Article

pubs.acs.org/IC

Room-Temperature Polar Order in $[NH_4][Cd(HCOO)_3]$ - A Hybrid Inorganic–Organic Compound with a Unique Perovskite Architecture

L. C. Gómez-Aguirre,[†] B. Pato-Doldán,[†] A. Stroppa,[‡] S. Yáñez-Vilar,[§] L. Bayarjargal,[∥] B. Winkler,[∥] S. Castro-García,[†] J. Mira,[§] M. Sánchez-Andújar,[†] and M. A. Señarís-Rodríguez*[,†]

[†]Department of Fundamental Chemistry, University of A Coruña, 15071, A Coruña, Spain

[‡]CNR-SPIN, 67100 L'Aquila, Italy

[§]Department of Applied Physics, University of Santiago de Compostela, 15782, Santiago de Compostela, Spain

[∥]Institute for Geoscience, University of Frankfurt, D-60438 Frankfurt a.M., Germany

Supporting Information

ABSTRACT: We report on the hybrid inorganic–organic ammonium compound $[NH_4][Cd(HCOO)_3]$, which displays a most unusual framework structure: instead of the expected $4^9{\cdot}6^6$ topology, it shows an ABX_3 perovskite architecture with the peculiarity and uniqueness (among all the up-to-date reported hybrid metal formates) that the Cd ions are connected only by *syn–anti* formate bridges, instead of *anti–anti* ones. This change of the coordination mode of the formate ligand is thus another variable that can provide new possibilities for tuning the properties of these versatile functional metal–organic framework materials. The room-temperature crystal structure of $[NH_4][Cd(HCOO)_3]$ is non-centrosymmetric (S.G.: $Pna2_1$) and displays a polar axis. DFT calculations and symmetry mode analysis show that the rather large polarization arising from the off-center shift of the ammonium cations in the cavities (4.33 $\mu C/cm^2$) is partially canceled by the antiparallel polarization coming from the $[Cd(HCOO)_3]^-$ framework, thus resulting in a net polarization of 1.35 $\mu C/cm^2$. As shown by second harmonic generation studies, this net polarization can be greatly increased by applying pressure (P_{max} = 14 GPa), an external stimulus that, in turn, induces the appearance of new structural phases, as confirmed by Raman spectroscopy.

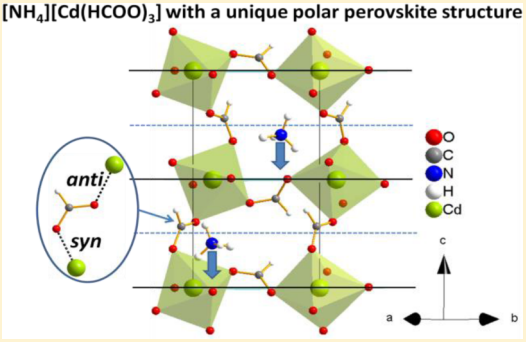

INTRODUCTION

Recent progress in metal–organic frameworks (MOFs) research has opened up new possibilities to achieve hybrid materials with a rich variety of functional and even multifunctional properties.[1−3] Among them, the subgroup of ABX_3 formate-based dense hybrids and, more particularly, the family where A are protonated amines ($AmineH^+$), B are divalent cations (M^{2+}), and X is the formate anion ($HCOO^-$), is particularly interesting in view of the dielectric,[4−6] magnetic,[7] magnetoelectric, and multiferroic properties[8−12] exhibited by some of its members.

From the structural point of view, all of these metal formate frameworks of the formula $[AmineH_n][M(HCOO)_3]$ (where $AmineH^+ = NH_4^+$, alkylammonium, arylammomnium, etc., and M^{2+} = B = divalent cations of transition metals, but also Mg^{2+}, Zn^{2+}, Cd^{2+}, etc.) consist of six-connected nodes of octahedral $[BO_6]$ units that are linked by bridging $HCOO^-$ anions, up to now, all in *anti–anti* coordination mode. The $AmineH_n^+$ cations are located in the resulting cavities and bonded to the framework via hydrogen bonds.[6,13,14]

The size of the protonated amines, cations that act as templates, is one of the factors that determine the structural topology of the resulting framework.[7,15] This aspect, together with the characteristics of M^{2+}, $AmineH^+$, and the coordination mode of the formate ligand, can play an important role on the dielectric, magnetic, and even multiferroic properties of the resulting materials.[4,16,17]

In this context, the presence of midsized alkylammonium cations, such as methylammonium, ethylammonium, dimethylammonium, hydrazinium, formamidinium, cyclotrimethyleneammonium, and imidazolium, leads to frameworks that have a perovskite architecture, where the metal cation has its six neighbors arranged in an octahedron, resulting in a $4^{12}{\cdot}6^3$ topology.[15,18−22] To this group belong the well-known dimethylammonium metal formates with a perovskite-like structure $[(CH_3)_2NH_2][M(HCOO)_3]$ (M^{2+} = Mg^{2+}, Mn^{2+}, Fe^{2+}, Co^{2+}, Ni^{2+}, and Zn^{2+}), which present electrical order below a T_t of 160–185 K in the case of the last five

Received: September 11, 2014
Published: February 9, 2015

DOI: 10.1021/ic502218n
Inorg. Chem. 2015, 54, 2109–2116

ones,[6,13,23−25] or even of 270 K (almost room temperature) when $M^{2+} = Mg^{2+}$.[26] In addition, such MOFs (except those of Zn^{2+} and Mg^{2+}) show multiferroic behavior,[13,27−30] as they also exhibit weak ferromagnetism at low temperatures (T_C = 8−36 K).[14,31,32]

Meanwhile, a small cation such as NH_4^+ gives rise to MOFs of the formula $[NH_4][M(HCOO)_3]$ ($M^{2+} = Mg^{2+}$, Mn^{2+}, Fe^{2+}, Co^{2+}, Ni^{2+}, and Zn^{2+}) and a different structural topology, namely, the chiral $4^9{\cdot}6^6$ one.[33−36] In this topology, the $[MO_6]$ octahedra are also six-connected but the coordination is trigonal prismatic instead of octahedral. Three prisms merge to form helical channels where the arrays of ammonium cations are located along the *c*-axis. Such ammonium formates present a spin-canted antiferromagnetic ordering below 8−30 K (depending on the specific M^{2+})[34] and an electric order below a certain T_t, which is associated with a decrease of the symmetry of the structure from $P6_322$ to $P6_3$.[33,35]

Very interestingly, the literature data on these $[NH_4][M(HCOO)_3]$ (M^{2+} = Mn^{2+}, Fe^{2+}, Co^{2+}, Ni^{2+}, and Zn^{2+}) compounds[33] reveal a direct correlation in this series between the size of the metal cation and T_t, which increases from 191 K for Zn^{2+} ($^{VI}\Gamma_{Zn^{2+}}$ = 0.74 Å) to 254 K for Mn^{2+} ($^{VI(HS)}\Gamma_{Mn^{2+}}$ = 0.83 Å).[37]

With the initial motivation of obtaining a material in which such an electrical order remains up to room temperature or above, rendering it more appropriate for technological applications, we decided to explore the effect of building the framework with an even larger M^{2+}cation. For this purpose, we selected the Cd^{2+} ion ($^{VI}\Gamma_{Cd^{2+}}$ = 0.95 Å), focusing on the resulting $[NH_4][Cd(HCOO)_3]$ compound.

In addition, we were also interested by the question of what happens from the structural point of view in these metal formates when the size mismatch between the protonated amine and the M^{2+} cation gets rather large, and this $[NH_4][Cd(HCOO)_3]$ formate could provide a good example.

In a previous short publication, Antsyshkina et al.[38] had reported a Cd-formate with that composition that, at room temperature, displayed a noncentrosymmetric structure (space group $Pn2_1a$). This means that potentially this compound could be ferroelectric, even if its dielectric/electrical properties had never been explored.

With that information and the above-mentioned 2-fold purpose, in this work, we synthesize the $[NH_4][Cd(HCOO)_3]$ formate and carry out a detailed study by means of single-crystal X-ray diffraction, density functional theory (DFT) calculations, ambient pressure and high-pressure nonlinear optics (second harmonic generation: SHG) measurements, and Raman spectroscopy.

As we will show below, the obtained results provide a deeper understanding of the different crystal structures displayed by the members of the family of ABX_3 formates as well as of the relationship between the crystal structure and the net polarization present in this $[NH_4][Cd(HCOO)_3]$ compound.

EXPERIMENTAL SECTION

Caution! *Compounds containing cadmium are highly toxic. Care must be taken when handling the samples, and appropriate disposal procedures are required.*

Materials. $Cd(ClO_4)_2{\cdot}xH_2O$ (Aldrich), $HCOONH_4$ (99.995%, Panreac), absolute methanol (99.5% Panreac), and formic acid (98%, Fluka) were commercially available and used as purchased without further purification.

Synthesis. For the synthesis, 4 mL of a methanol solution containing 0.10 M $Cd(ClO_4)_2{\cdot}xH_2O$ was placed at the bottom of a glass tube. Upon the Cd^{2+} solution, 4 mL of a methanol solution containing 0.80 M $HCOONH_4$ and 0.40 M HCOOH was carefully layered; the tube was sealed and kept undisturbed. Colorless crystals with a plate morphology were obtained after 2 weeks. They were washed with ethanol and dried at room temperature.

Elemental Analysis. Elemental chemical analyses for C, N, and H were carried out using a FlashEA1112 (ThermoFinnigan) Analyzer.

For this compound: calculated: C: 13.57, H: 2.65, N: 5.27; found: C: 13.59, H: 2.49, N: 5.45.

Single-Crystal X-ray Diffraction. Single-crystal data sets were collected at 350, 295, and 100 K with a Bruker-Nonius x8 ApexII X-ray diffractometer equipped with a CCD detector and using monochromatic Mo$K\alpha_1$ radiation (λ = 0.71073 Å). For that purpose, a suitable crystal was chosen and mounted on a glass fibber using instant glue. The data integration and reduction was performed using the Apex2 V.1.0-27 (BrukerNonius, 2005) suite software. The intensity collected was corrected for Lorentz and polarization effects and for absorption by semiempirical methods on the basis of symmetry-equivalent data using SADABS (2004) of the suite software. The structure was solved by the direct method using the SHELXS-97[39] program and was refined by least-squares method on SHELXL-97.[40] Anisotropic thermal factors were employed for the non-H atoms. The hydrogen atoms of the formate and ammonium cation were found in the Fourier map, and their coordinates and isotropic thermal factors were refined.

Powder X-ray Diffraction. Powder X-ray diffraction (PXRD) at room temperature was performed in a Siemens D-5000 diffractometer using Cu$K\alpha$ radiation (λ = 1.5418 Å). The obtained PXRD patterns were analyzed by Le Bail profile analysis using the Rietica software.[41] The peak shapes were described by a pseudo-Voigt function, and the background was modeled with a 6-term polynomial function.

Thermal Studies. Thermogravimetric analyses (TGA) were carried out in a TGA-DTA Thermal Analysis SDT2960 equipment. For these experiments, approximately 27 mg of sample was heated at a rate of 5 K/min from 300 to 800 K using corundum crucibles under a flow of dry nitrogen.

Differential scanning calorimetric (DSC) analyses were carried out in a TA Instruments MDSC Q-2000 equipped with a liquid nitrogen cooling system, by heating and cooling the sample $[NH_4][Cd(HCOO)_3]$ during several cycles at 10 K/min from 270 K up to 370 K under a nitrogen atmosphere.

Ambient Conditions and High-Pressure Experiments Using Second Harmonic Generation and Raman Spectroscopy. Sample preparation: A powdered sample of $[NH_4][Cd(HCOO)_3]$ was loaded in Boehler-Almax[42] type diamond anvil cells (DACs). Holes of about 120 μm in diameter were drilled into preindented (to 40−50 μm thickness) tungsten gaskets and served as sample chambers. Small pieces of ruby were loaded for pressure determination using the ruby fluorescence. Argon and neon were used as a pressure medium for the second harmonic generation (SHG) experiments and Raman spectroscopy, respectively.

SHG experiments were performed on the powdered samples at pressures between 1 atm and 21.4 GPa using a pulsed Nd:YLF (Falcon 217D, Quantronix) laser at 1054 nm. With a harmonic separator, a short-pass filter, and an interference filter, the fundamental infrared light was separated from the generated second harmonic. The generated SHG signal (527 nm) was collected with a photomultiplier (R2949, Hamamatsu) and photon counter (SRS400). At each pressure point, 15−30 measurements were performed and the average value was calculated. Quartz (α-SiO_2) and Al_2O_3 powder were used as reference materials.

Confocal micro-Raman measurements at ambient pressure and high pressure were carried out with a Renishaw Raman spectrometer (RM-100) equipped with a Leica DMLM optical microscope with a grating with 1800 grooves per mm and a Peltier-cooled charge-coupled device (CCD). For excitation, the 532 nm line of a Nd:YAG laser with a power of 20 mW was used. A 20× objective lens with a long working distance and a quasi-backscattering geometry was employed. The spectra were collected in the range of 100−3200 cm^{-1} with exposure times of 60 s at different pressures up to 20 GPa. The system was

DOI: 10.1021/ic502218n
Inorg. Chem. 2015, 54, 2109−2116

calibrated using the band at 519 cm^{-1} of a Si wafer. The collected spectra were corrected by subtracting the background and fitted using Lorentzian-type functions. The accuracy of the wavenumbers was ≈1 cm^{-1}, and the spectral resolution was 2 cm^{-1}.

Density Functional Calculations and Symmetry Analysis. DFT calculations combined with symmetry mode analysis have been performed using the Vienna Ab initio Simulation Package (VASP),[43,44] using the projector augmented-wave (PAW) method with the Perdew–Burke–Ernzerhof (PBE) GGA functional. The energy cutoff was set to 400 eV, and a 6 × 4 × 4 Monkhorst–Pack grid of *k*-points was used. The Berry phase approach was employed to calculate the ferroelectric polarization.[45]

Starting from the low symmetry structure, we introduced a reference centric structure that mimics a displacive type phase transition between the paraelectric and polar structure. Although the real nature of the phase transition must be ascribed to order–disorder type, this approach is useful for evaluating the polarization using ab initio methods. The low symmetry structure can be obtained from the reference structure by small atomic displacements. In this case, the high symmetry (reference) structure is said to be pseudosymmetric to the low symmetry structure. It is important to note that the reference structure is only a computational tool for evaluating the polarization and, in general, it does not need to be a "real" paraelectric structure. For instance, it may be used in the computations instead of a real disordered paraelectric structure, which would be difficult to simulate. From a physical point of view, the approach is well justified since the estimated polarization does not depend on the choice of the reference paraelectric structure, since, by symmetry, it has zero net polarization. Furthermore, by considering an ordered centric structure instead of a disordered one, one can use distortion mode analysis in order to analyze the displacement leading to the polar structure (symmetry mode analysis).

RESULTS AND DISCUSSION

Synthesis and Basic Characterization. We have prepared both single crystals and polycrystalline samples of $[NH_4][Cd(HCOO)_3]$ by adapting the solution diffusion method reported for the preparation of $[NH_4][Zn(HCOO)_3]$,[35] where the synthesis is accomplished through mild solution chemistry at ambient temperature.

We have confirmed the purity of the prepared sample by LeBail refinement[46] of the PXRD data obtained at room temperature, which show good agreement between the experimental data and the model (Figure S1 of the Supporting Information).

This $[NH_4][Cd(HCOO)_3]$ formate is stable only up to 373 K according to our TGA results (Figure S2 of the Supporting Information). Above that temperature, it decomposes in several steps of weight loss, the first one corresponding to the loss of the NH_4^+ cations and one of the $HCOO^-$ anions (see more details in Figure S2).

Up to 373 K, the compound does not experience any phase transition, as indicated by the DSC results (see Figure S3 of the Supporting Information), and the single crystal data obtained at three different temperatures, namely 100, 298, and 350 K (see below). Concerning the former, it should be indicated that the broad endothermic peak that appears in the DSC curve around 325 K when the sample is heated for the first time is merely due to the elimination of moisture present at the surface of the crystals, and not to a structural transformation: the sample presents the same crystal structure above and below that temperature, as revealed by single-crystal X-ray diffraction. Once such moisture is eliminated from the sample, no further peak is observed neither on cooling nor on heating again the sample up to its decomposition temperature.

Crystal Structure. Our single-crystal X-ray studies unambiguously indicate that this compound maintains the same crystal structure from 100 K up to at least 350 K: its structure remains orthorhombic with cell parameters at room temperature: a = 6.9888(2) Å, b = 9.4902(2) Å, c = 10.8342(3) Å, values that are seen to slightly increase not only at higher temperature (350 K) but also more unexpectedly at lower temperature (100 K). Its space group is the noncentrosymmetric $Pna2_1$, which is coincident with that previously attributed to this compound,[38] but we prefer a setting where $a < b < c$ so that the polar axis is parallel to c.

This crystal structure whose asymmetric unit contains one independent Cd^{2+} cation, three $HCOO^-$ formate groups bound to the metal cation, and one NH_4^+ entity is shown in Figure 1

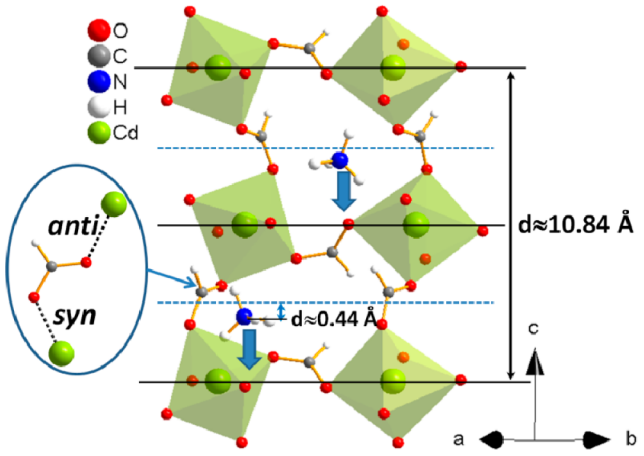

Figure 1. Crystal view of $[NH_4][Cd(HCOO)_3]$ highlighting the *syn–anti* coordination mode of the bridging formate and the cooperative off-center shift of the NH_4^+ cations along the polar *c*-axis. The black solid lines show the metal planes along the [001] direction, while the blue dashed lines indicate those where the A cations would be located in the centric structure.

and Figures S3–S6 of the Supporting Information. As can be seen, it consists of highly distorted $[CdO_6]$ octahedra, where the Cd^{2+} ions are connected to their six nearest neighbor metals through six formate bridges in a *syn–anti* conformation and with the ammonium ions located inside the cavities. The corresponding structural data are summarized in Table 1 and Table SI of the Supporting Information.

These results show that this Cd-formate displays a distorted perovskite-like architecture with topological structure $4^{12}\cdot6^3$, in contrast to the other members of the ammonium series of compounds $[NH_4][M(HCOO)_3]$ (M^{2+} = Mg^{2+}, Mn^{2+}, Fe^{2+}, Co^{2+}, Ni^{2+}, and Zn^{2+}).

Such a topology is indeed similar to that shown by the perovskite-like formates formed with midsized alkylammonium cations.

However, the peculiarity and uniqueness of the structure shown here as compared to that of all the up to now reported ABX_3-hybrid metal formates with a perovskite architecture relies in the fact that the metal centers are connected by bridging $HCOO^-$ anions, that all and only display a *syn–anti* coordination mode (see Figure 1).

In that regard, it should be mentioned that there are a couple of examples of ABX_3-formates where the formate ligand is known to adopt such a coordination mode, such as $K[M(HCOO)_3]$ (where M^{2+} = Mn^{2+}, Co^{2+}, and Cd^{2+})[38,47,48] or

DOI: 10.1021/ic502218n
Inorg. Chem. 2015, 54, 2109–2116

Table 1. Data Collection, Cell and Refinement Parameters from the Single-Crystal X-ray Diffraction Study Carried Out at T = 100 K, T = 295 K, and at T = 350 K

	T = 100 K	T = 295 K	T = 350 K
a/Å	6.9949(1)	6.9888(2)	7.0025(3)
b/Å	9.5029(2)	9.4902(2)	9.5060(4)
c/Å	10.8457(2)	10.8342(3)	10.9003(5)
unit cell volume/Å^3	720.93(2)	718.58(3)	725.59(5)
space group	$Pna2_1$	$Pna2_1$	$Pna2_1$
Z	4	4	4
radiation type	MoKα	MoKα	MoKα
no. of reflections measured	8833	15 874	34 242
no. of independent reflections	1816	2134	3520
R_{int}	0.0273	0.0283	0.0485
final R1 values ($I > 2\sigma(I)$)	0.0162	0.0166	0.0343
final wR (F^2) values ($I > 2\sigma(I)$)	0.0372	0.0367	0.0824
final R1 values (all data)	0.0172	0.0174	0.0409
final wR (F^2) values (all data)	0.0378	0.0371	0.0870
goodness of fit on F^2	1.121	1.088	0.996
Flack parameter	−0.02(3)	0.03(3)	0.03(4)

$Na[Mn(HCOO)_3]$,[49] but there are significant differences with this case. The $K[M(HCOO)_3]$ compounds show a perovskite-like architecture, but where the transition metal cations are linked by four equatorial *syn*−*anti* $HCOO^-$ groups and two axial *anti*−*anti* bridging ones;[47] that is, the formate ions present the two coordination modes. Meanwhile, in the case of the sodium compound, even if the metal centers are only coordinated by *syn*−*anti* HCOO-bridges, the structure is no longer a perovskite-like but a structure with $3^3{\cdot}5^6$ topology.[49]

This finding brings us to the question of under which circumstances the formate ligands prefer the *syn*−*anti* coordination mode over the *anti*−*anti* one in these compounds.

In that context, it is known that, in the perovskite-like formates formed with midsized alkylammonium cations, all the formate ions display an *anti*−*anti* coordination mode. In addition, in a recent work of Kieslich et al.[50] that extends the classical concept of ionic tolerance factor to hybrid phases, the authors conclude that these compounds show a perovskite-type structure because their tolerance factor (α) is above a certain value, which they estimate to be around 0.81.[50] Such relative high tolerance factors, in turn, mean that the sizes of the A and B cations match rather well, making this structural type favorable. Also, according to these authors, further decrease below that α value will favor a different structure. On the basis of the examples they have analyzed (formates with midsize protonated amines or with ammonium in the A site and with only *anti*−*anti* $HCOO^-$ bridges), they conclude that it will be the chiral hexagonal structure with $4^9{\cdot}6^6$ topological structure.

If using the same method we calculate now the tolerance factor for this Cd-formate $[NH_4][Cd(HCOO)_3]$, we come to a considerable smaller tolerance factor value: α = 0.62. If we do the same with the formate compounds $K[M(HCOO)_3]$ with M^{2+} = Mn^{2+}, Co^{2+}, and Cd^{2+}, we also come to values below 0.81 (α between 0.64 and 0.70), even if higher than in the case of the Cd compound.

This means that, upon a further decrease of the tolerance factor by reducing the size of the A cation and/or increasing the size of the B cation, below a certain value, the perovskite structure can be again stabilized by changing the coordination mode of the formate ion. This is possibly because this variable allows spreading out, shrinking, and/or modifing the shape of the cavity where the A cation is located (Figure S6, Supporting Information). Therefore, the change in the coordination mode of $HCOO^-$ helps to a better matching of the sizes of the A and B cations and their better interaction with the framework.

Nevertheless, the mentioned case of the $Na[Mn(HCOO)_3]$ compound (with α = 0.59) indicates that there is also a lower limit for the tolerance factor, below which the perovskite structure is no longer supported and a different phase forms.

With these data, the picture of possible structures that can present the ABX_3-formates as a function of the tolerance factor should be enlarged (see Figure 2). In addition to the perovskite

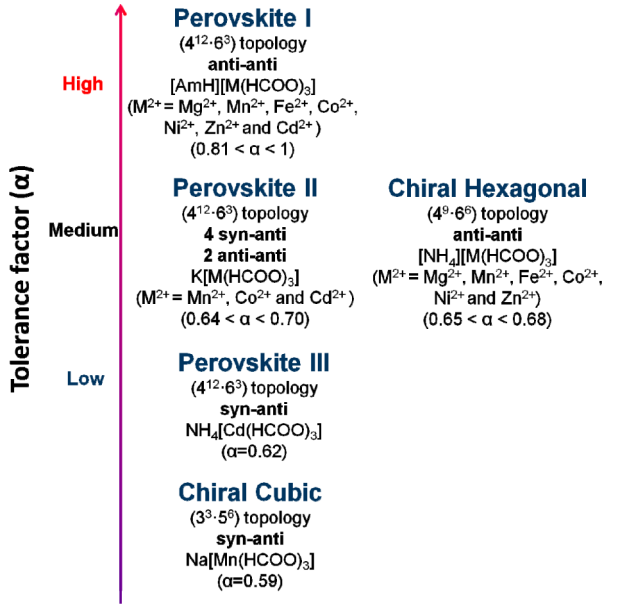

Figure 2. Evolution of the crystal structure of ABX_3-formates and the coordination modes of the X formate anions as a function of the tolerance factor (α).

type-I structure containing all formate ions in *anti*−*anti* coordination mode (displayed by hybrid formates with high tolerance factor), and the chiral one with $4^9{\cdot}6^6$ topology,[50] two more should be included: namely, a perovskite type-II structure, where the metal centers are coordinated by four formate ligands in a *syn*−*anti* mode and two in an *anti*−*anti* mode (for middle-tolerance factor values), and a perovskite type-III structure where all the formate ligands display a *syn*−*anti* coordination mode (for low tolerance factors). For even lower tolerance factors, the $3^3{\cdot}5^6$ topology gets favored instead of the perovskite one.

Among other questions that remain to be clarified are the exact tolerance factor limits for the appearance of the different phases and when and why different phases can be favored over the perovskite one, for example, the chiral ones, even if the presence and possibility of stronger hydrogen bonds not mentioned in the above discussion could also be playing an important role. Some of these phases seem to have a relatively close energy in view of the polymorphism presented by compounds such as $K[Co(HCOO)_3]$, with either a perovskite structure or the chiral one with $4^9{\cdot}6^6$ topology.[47]

The $[NH_4][Cd(HCOO)_3]$ compound thus represents the first member of a new family of formate compounds, where the presence of only *syn*−*anti* formate bridges can lead to different $[MO_6]$ octahedra tiltings, that leave cavities of different sizes

DOI: 10.1021/ic502218n
Inorg. Chem. 2015, 54, 2109−2116

and shapes, to different metal−metal interactions, etc. Most interestingly, this, in turn, implies new possibilities for tuning further the functional properties of these versatile MOF materials.

Coming back to the description of the $[NH_4][Cd(HCOO)_3]$ structure, there is another aspect that is worth highlighting and that concerns the ammonium cation.

This A cation is located inside the highly distorted cavity created by the $[Cd(HCOO_3)]^-$ framework with whom it is bonded through four H bonds between its N atom and the O atom of formate anions (see Figure S4 of the Supporting Information [d(N−H···O) = 2.07(4)−2.34(4) Å at room temperature, Table SI]). Most interestingly, the position of the ammonium cations is shifted off-center inside the cavity by about 0.44 Å (Figure 1 and Figures S5 and S6 of the Supporting Information), a shift that is of the same order as that reported for the other members of the $[NH_4][M(HCOO)_3]$ series with M = Mn^{2+}, Fe^{2+}, Co^{2+}, Ni^{2+}, and Zn^{2+}, which ranges from 0.359(7) to 0.482(4) Å.[33] This displacement of the ammonium cations inside the cavities is cooperative with all of them moving off-center along the same direction (the polar c-axis).

Due to this off-center shift, the distances between the Cd^{2+} ions and the N atoms of the ammonium cations differ significantly from each other, with the shortest bond length being about 3.80 Å and the largest one about 6.96 Å (see Table SI of the Supporting Information).

DFT Calculations. In view of the polar structure displayed by this $[NH_4][Cd(HCOO)_3]$ compound, we have explored the possibility that it shows cooperative electrical order by DFT calculations.

For this purpose, we considered a centric reference structure with space group *Pnma*.[51,52] The low symmetry $Pna2_1$ structure can be obtained from the centric structure by a polar $GM5^-$ distortion mode. Note that the choice of the reference centric structure does not influence the final polarization value. In fact, another possible choice of a reference structure would differ by a $GM1^+$ mode, which preserves the inversion center, and thus it would not contribute to the polarization.

Figure 3 shows the displacement vector field superimposed on the reference centric structure where the lengths of the vectors are proportional to the corresponding atomic displacement with respect to the centric phase.

From our results, it is clear how large atomic displacements affect the oxygen and carbon atoms of the organic ligands. They are mainly localized in the plane perpendicular to the polar axis, and they largely compensate and do not contribute to the overall polarization. On the other hand, large atomic displacements affect the H atoms of the carboxylate ligand and they are localized along the polar direction. However, the distortions of the $[BO_6]$ octahedra as well as of the organic ligands of the BX_3 framework have also a component along the polar axis. (see discussion below). Small displacements are affecting also the H atoms of the ammonium cation, mainly along the polar axis. The total estimated polarization from the DFT calculations is 1.35 $\mu C/cm^2$.

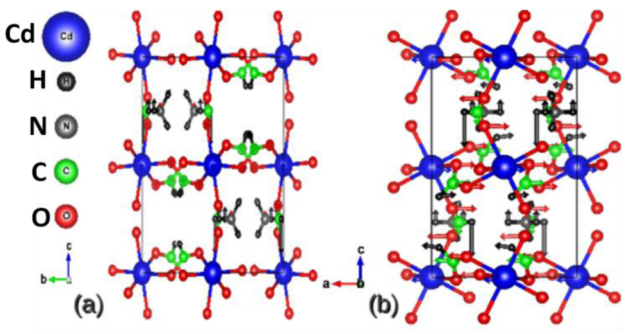

Figure 3. Atomic displacement field superposed on the reference centric structure. (a) is a projection along [100]. (b) shows a projection along [010]. Lengths of vectors are proportional to the corresponding atomic displacement.

It is also useful to perform a functional group analysis of the polarization, i.e., to decompose the polarization into contributions coming from the different functional units such as $[NH_4]^+$, Cd^{2+}, and $HCOO^-$, i.e., the A cation, B metal atom, and X ligand of this ABX_3 compound. This can be done by comparing the polar structure with $Pna2_1$ symmetry with the reference paraelectric structure and by calculating the polarization when moving only the atoms belonging to a given functional group while keeping all the other atoms in their centrosymmetric positions. The contribution from the dipole moment of the A group is then P_A = (0,0,4.33) $\mu C/cm^2$. Although the contribution to the polarization by the organic cation seems to be large, it is considerably reduced by a depolarization effect of the BX_3 framework, leaving a much smaller net polarization.

Ambient Conditions and High-Pressure Experiments Using Second Harmonic Generation and Raman Spectroscopy. We have performed SHG experiments not only to experimentally confirm the occurrence of ferro-/ferrielectricity at room temperature in $[NH_4][Cd(HCOO)_3]$, but also to explore the influence of external pressure on the net polarization of this compound. In this context, it is known that the zinc analogue $[NH_4][Zn(HCOO)_3]$, with $4^9{\cdot}6^6$ topology, exhibits negative linear compressibility.[53] Also, we have recently reported that, in the case of the dimethylammonium Mn-formate $[(CH_3)_2NH_2][Mn(HCOO)_3]$ with perovskite-like structure, T_t displays a large pressure dependence due to its rather "soft" nature.[54]

In the present case of $[NH_4][Cd(HCOO)_3]$, it can be expected that externally applied pressure will greatly affect the polarization, due to the strong correlation found between its crystal structure and the polarization.

In initial experiments, carried out at ambient conditions, and in the absence of applied pressure, the SHG signal of Cd-formate was about 2 times stronger than that of quartz. The average SHG value $d^{SHG}_{av} = \chi^{(2)}_{av}/2$ = 0.6 pm/V, a value that is slightly higher than that displayed by the ferroelectric metal formate compounds, $[(CH_3)_2NH_2][M(HCOO)_3]$ (M^{2+} = Mn^{2+}, Co^{2+}, Zn^{2+})[4], where $\chi^{(2)}_{av}/2$ = 0.2−0.4 pm/V or by the other metal formates, such as $Y(HCOO)_3{\cdot}2H_2O$[55] and $M(HCOO)_2$ (M^{2+}= Sr^{2+}, Ba^{2+}).[56,57]

Further experiments were subsequently performed by applying pressure to the sample.

There is a clear pressure dependence of the room-temperature SHG intensity (Figure 4). The precision with which SHG signal intensities can be determined in a diamond anvil cell is limited. However, our observations (Figure 4) suggest that there are phase transitions around 1.4 and 5 GPa, and a further phase transition at 14 GPa. While at lower pressures (around 5 GPa), the SHG intensity is small, it is always at least 8 times higher than that of a centrosymmetric Al_2O_3 reference crystal, so that we can safely conclude that the

DOI: 10.1021/ic502218n
Inorg. Chem. 2015, 54, 2109−2116

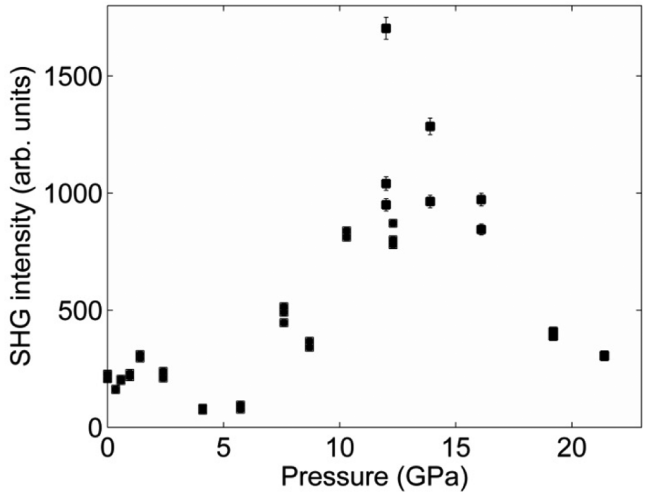

Figure 4. Pressure dependence of the ambient temperature SHG intensity of $[NH_4][Cd(HCOO)_3]$.

structure remains acentric up to the highest pressures investigated.

Furthermore, a positive pressure dependence of the SHG intensity is possible only in nonphase matchable crystals.[58] Therefore, we can conclude that $[NH_4][Cd(HCOO)_3]$ is nonphase matchable between 0 and 1.4 GPa and 5−14 GPa.

Very interestingly, upon application of pressures between 4.8 and 14 GPa, (Figure 4), the SHG signal is seen to reach a maximum value at around 14 GPa, which is about 6 times higher than the one observed at ambient pressure. Higher pressures exceeding 14 GPa result in an opposite pressure dependence where the SHG intensity decreases with increasing pressure.

In summary, the results obtained here show not only that the SHG signal is strongly pressure dependent but also that the polar character of $[NH_4][Cd(HCOO)_3]$ can be greatly enhanced by applying pressure.

To proof the possible occurrence of the phase transitions suggested by the SHG experiments, we have recorded the Raman spectra of this compound as a function of pressure up to 20 GPa.

As it is known, the vibrational spectra of $[NH_4][Cd(HCOO)_3]$ consist basically in the internal vibrations of the ammonium and formate ions, and the lattice vibrations. At ambient pressure, the bands observed in the region of 800−3800 cm^{-1} are characteristic for the internal modes of NH_4^+ and COO^- groups, while those observed below 400 cm^{-1} correspond usually to lattice modes.[59,60]

Upon application of pressure, significant changes occur, as it can be seen in some selected examples shown in Figures 5a,b and Figure S7 of the Supporting Information. In that context, five groups of spectra can be distinguished: Group I, for initially low pressures up to 1.6 GPa, where the spectra remain qualitatively the same with the wavenumber of the majority of the modes increasing with pressure, and Group II ($2.6 \leq P$ (GPa) ≤ 5.5), Group III ($P = 8.7$ GPa), Group IV ($10.5 \leq P$ (GPa) ≤ 14.0), and Group V ($15.5 \leq P$ (GPa) ≤ 19.9), which differ from one another in discontinuous wavenumber shifts, changes in the slope of wavenumber versus pressure, splitting of internal modes into doublets or even triplets, and a change in the intensity of many bands. The observed modifications of the Raman spectra give evidence for three clear phase transitions

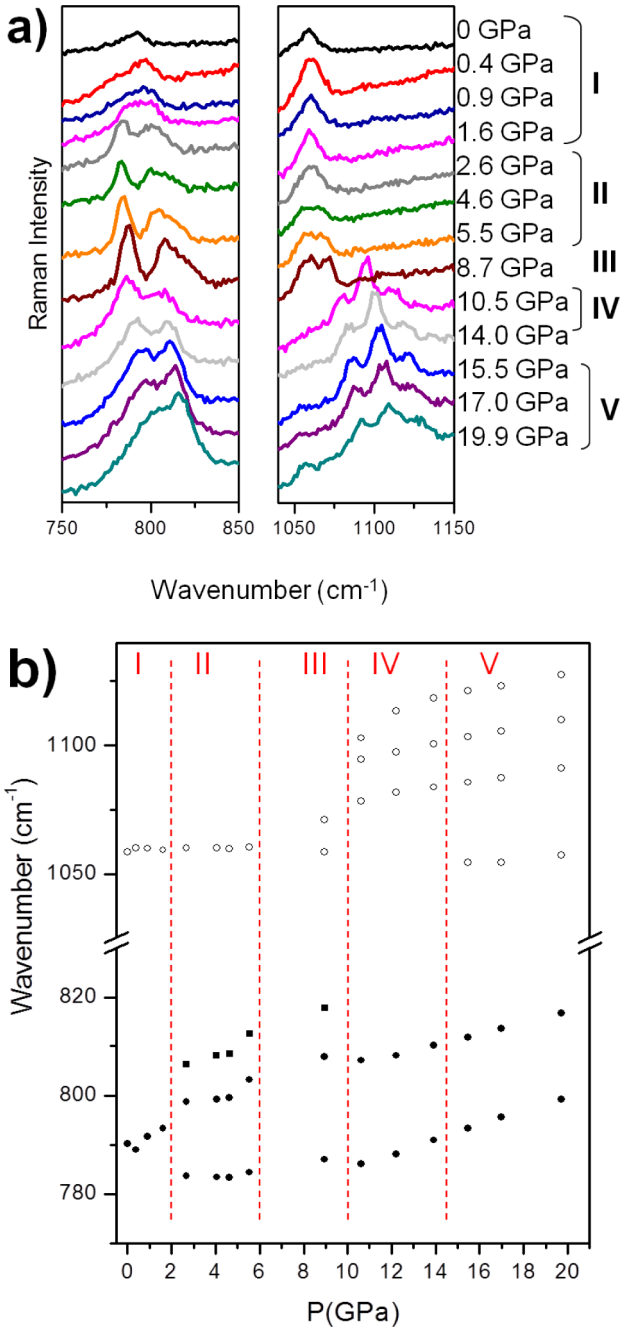

Figure 5. (a) Detail of the Raman spectra corresponding to the spectral ranges of 750−850 and 1040−1150 cm^{-1}. (b) Wavenumber vs pressure plots of the Raman modes corresponding to ν_3 ($HCOO_3^-$) (symmetric O-C-O bending) and ν_6 ($HCOO_3^-$) (out of plane H-C mode), represented as closed and open circles, respectively. The vertical lines signal approximate pressures at which the phase transitions take place.

occurring at around 2.5, 6, and 10 GPa, and an additional more subtle one taking place at around 14 GPa, in agreement with the SHG results. The small differences of transition pressures might be coming from the different pressure media in SHG and Raman experiments, and the observed splitting of the internal modes point to lower symmetry of the high-pressure phases as compared to the ambient one.

Very interestingly, the pressure-induced phase transitions bring about a strong distortion of the anionic framework, in

DOI: 10.1021/ic502218n
Inorg. Chem. 2015, 54, 2109−2116

view of the strong pressure dependence of the O-C-O bending mode ($\nu_6(HCOO^-)$) and the out-of-plane H-C mode ($\nu_6(HCOO_3^-)$) (see Figure 5a,b), and the lattice modes. It also has a marked influence on the NH_4^+ cations, whose vibrational modes experience a very pronounced shifting toward the blue (Figure S7 of the Supporting Information), much larger than in the case of the related Mg and Zn compounds $[NH_4][M(HCOO)_3]$.[61,62] This result reveals a significant weakening upon application of pressure of the initially robust N−H···O hydrogen−bonds between the ammonium cations and the framework, which is probably related to shifts of the NH_4^+ cation inside the cavity.

In any case, and even if the structural modifications upon pressure application are large, the structure of the high-pressure phases probably does not differ drastically from that of the original parent phase as the original structure can be recovered by decompression after the sample has been subjected to the highest pressure.

SHG and Raman results indicate that the pressure-induced change of the polarization can be caused by the pressure-induced shift of the A cation (NH_4^+) and the distortions of the $[Cd(HCOO)_3]^-$ framework, which are affecting the values of the initially antiparallel electrical dipoles by diminishing their partial cancellation in the case of phases I and III, IV (thus resulting in a higher net polarization), while favoring their cancellation in phases II and V.

CONCLUSIONS

By single-crystal X-ray diffraction, DFT calculations, nonlinear optical measurements (SHG), and Raman spectroscopy, we have studied $[NH_4][Cd(HCOO)_3]$, a compound that displays a new crystal structure that is different from that of the other members of the $[NH_4][M(HCOO)_3]$ series (with M^{2+} = Mg^{2+}, Mn^{2+}, Fe^{2+}, Co^{2+}, Ni^{2+}, and Zn^{2+}). In this Cd-formate, the $[Cd(HCOO)_3]^-$ framework shows a $4^{12}\cdot6^3$ topology and a perovskite architecture, but with the peculiarity and uniqueness among all the so far described hybrid metal formates with a perovskite structure that the metal centers are all and only connected by *syn*−*anti* bridging formate anions, instead of conventional *anti*−*anti* formate bridges.

This compound, with a rather low tolerance factor of α = 0.62, exemplifies another variable by which the perovskite structure can be stabilized and the properties of these versatile functional MOF materials can be tuned: by making use of the change of the coordination mode of the formate ion, possibility that does not exist in the oxides and halides perovskites.

The room-temperature crystal structure of $[NH_4][Cd(HCOO)_3]$ is noncentrosymmetric (S.G.: $Pna2_1$) and possesses a polar axis. According to density functional theory and symmetry mode analysis, this compound displays a net polarization of 1.35 $\mu C/cm^2$, a value that is lower than the polarization arising from just the off-center shift of the ammonium cation in the cavities (4.33 $\mu C/cm^2$) as it is partially canceled by the antiparallel polarization coming from the $[Cd(HCOO)_3]^-$ framework. The presence of a net electrical polarization was confirmed by SHG studies, which also showed that it can be greatly increased by external pressures up to 14 GPa.

The application of pressure up to 20 GPa induces three clear phase transitions, and a fourth more subtle one, that lead to different high-pressure phases, as initially suggested by the SHG experiments and confirmed by Raman spectroscopy experiments carried out under pressure.

The detailed characterization of the higher-pressure phases of this compound is now in progress even if their full description will be rather challenging. Other characterization techniques such as synchrotron X-ray powder diffraction cannot be used, in view of our preliminary attempt carried out at 10.8 GPa at the Extreme Conditions Beamline P02.2 in Hamburg, which showed that the compound is too sensitive to the high intensity X-ray radiation required.

ASSOCIATED CONTENT

Supporting Information

An X-ray crystallographic file (CIF). LeBail refinement of the PXRD pattern, thermogravimetric curve, crystal structure views, and table of bond lengths. This material is available free of charge via the Internet at http://pubs.acs.org.

AUTHOR INFORMATION

Corresponding Author

*Fax: +34981167065. Tel: +34981167000. E-mail: m.senaris.rodriguez@udc.es (M.A.S.-R.).

Notes

The authors declare no competing financial interest.

ACKNOWLEDGMENTS

The authors are grateful for financial support from Ministerio de Economía y Competitividad (MINECO) (Spain) and EU under the project FEDER MAT2010-21342-C02-01, and Xunta de Galicia under the project GRC2014/042. A.S. acknowledges discussions with J. M. Perez-Mato. In this case, the polarization would not have been easily calculated without the use of the tools of the Bilbao Crystallographic Server. S.Y−V. acknowledges Xunta de Galicia for a *Postdoctoral* fellowship.

REFERENCES

(1) Yaghi, O. M.; Guangming, L.; Hailian, L. *Nature* **1995**, *378*, 703−706.
(2) Cheetham, A. K.; Rao, C. N. R. *Science* **2007**, *318*, 58−59.
(3) Pardo, E.; Train, C.; Liu, H.; Chamoreau, L.-M.; Dkhil, B.; Boubekeur, K.; Lloret, F.; Nakatani, K.; Tokoro, H.; Ohkoshi, S.; Verdaguer, M. *Angew. Chem.,Int. Ed.* **2012**, *51*, 8356−8360.
(4) Zhang, W.; Xiong, R.-G. *Chem. Rev.* **2012**, *112*, 1163−1195.
(5) Hang, T.; Zhang, W.; Ye, H.-Y.; Xiong, R.-G. *Chem. Soc. Rev.* **2011**, *40*, 3577−3598.
(6) Jain, P.; Dalal, N. S.; Toby, B. H.; Kroto, H. W.; Cheetham, A. K. *J. Am. Chem. Soc.* **2008**, *130*, 10450−10451.
(7) Wang, Z.; Hu, K.; Gao, S.; Kobayashi, H. *Adv. Mater.* **2010**, *22*, 1526−1533.
(8) Rogez, G.; Viart, N.; Drillon, M. *Angew. Chem., Int. Ed.* **2010**, *49*, 1921−1923.
(9) Stroppa, A.; Jain, P.; Barone, P.; Marsman, M.; Perez-Mato, J. M.; Cheetham, A. K.; Kroto, H. W.; Picozzi, S. *Angew. Chem., Int. Ed.* **2011**, *50*, 5847−5850.
(10) Stroppa, A.; Barone, P.; Jain, P.; Perez-Mato, J. M.; Picozzi, S. *Adv. Mater.* **2013**, *25*, 2284−2290.
(11) Cañadillas-Delgado, L.; Fabelo, O.; Rodríguez-Velamazán, J. A.; Lemée-Cailleau, M.-H.; Mason, S. A.; Pardo, E.; Lloret, F.; Zhao, J.-P.; Bu, X.-H.; Simonet, V.; Colin, C. V.; Rodríguez-Carvajal, J. *J. Am. Chem. Soc.* **2012**, *134*, 19772−19781.
(12) Wang, W.; Yan, L.-Q.; Cong, J.-Z.; Zhao, Y.-L.; Wang, F.; Shen, S.-P.; Zou, T.; Zhang, D.; Wang, S.-G.; Han, X.-F.; Sun, Y. *Sci. Rep.* **2013**, *3*, 1−5.
(13) Jain, P.; Ramachandran, V.; Clark, R. J.; Zhou, H. D.; Toby, B. H.; Dalal, N. S.; Kroto, H. W.; Cheetham, A. K. *J. Am. Chem. Soc.* **2009**, *131*, 13625−13627.

DOI: 10.1021/ic502218n
Inorg. Chem. 2015, 54, 2109−2116

(14) Wang, X.-Y.; Gan, L.; Zhang, S.-W.; Gao, S. *Inorg. Chem.* **2004**, *43*, 4615−4625.
(15) Wang, Z.; Zhang, B.; Otsuka, T.; Inoue, K.; Kobayashi, H.; Kurmoo, M. *Dalt. Trans.* **2004**, 2209−2216.
(16) Di Sante, D.; Stroppa, A.; Jain, P.; Picozzi, S. *J. Am. Chem. Soc.* **2013**, *135*, 18126−18130.
(17) Weng, D.; Wang, Z.; Gao, S. *Chem. Soc. Rev.* **2011**, *40*, 3157−3181.
(18) Hu, K.-L.; Kurmoo, M.; Wang, Z.; Gao, S. *Chem.—Eur. J.* **2009**, *15*, 12050−12064.
(19) Mączka, M.; Ciupa, A.; Gągor, A.; Sieradzki, A.; Pikul, A.; Macalik, B.; Drozd, M. *Inorg. Chem.* **2014**, *53*, 5260−5268.
(20) Chen, S.; Shang, R.; Hu, K.-L.; Wang, Z.-M.; Gao, S. *Inorg. Chem. Front.* **2014**, *1*, 83−98.
(21) Shang, R.; Xu, G.-C.; Wang, Z.-M.; Gao, S. *Chem.—Eur. J.* **2014**, *20*, 1146−1158.
(22) Pato-Doldán, B.; Gómez-Aguirre, L. C.; Bermúdez-García, J. M.; Sánchez-Andújar, M.; Fondado, A.; Mira, J.; Castro-García, S.; Señarís-Rodríguez, M. A. *RSC Adv.* **2013**, *3*, 22404−22411.
(23) Sánchez-Andújar, M.; Presedo, S.; Yáñez-Vilar, S.; Castro-García, S.; Shamir, J.; Señarís-Rodríguez, M. A. *Inorg. Chem.* **2010**, *49*, 1510−1516.
(24) Besara, T.; Jain, P.; Dalal, N. S.; Kuhns, P. L.; Reyes, A. P.; Kroto, H. W.; Cheetham, A. K. *Proc. Natl. Acad. Sci. U.S.A.* **2011**, *108*, 6828−6832.
(25) Mączka, M.; Ptak, M.; Macalik, L. *Vib. Spectrosc.* **2014**, *71*, 98−104.
(26) Pato-Doldán, B.; Sánchez-Andújar, M.; Gómez-Aguirre, C.; Yáñez-Vilar, S.; López-Beceiro, J.; Gracia-Fernández, C.; Haghighirad, A. A.; Ritter, F.; Castro-García, S.; Señarís-Rodríguez, M. A. *Phys. Chem. Chem. Phys.* **2012**, *14*, 8498−8501.
(27) Fu, D.-W.; Zhang, W.; Cai, H.-L.; Zhang, Y.; Ge, J.-Z.; Xiong, R.-G.; Huang, S. D.; Nakamura, T. *Angew. Chem., Int. Ed.* **2011**, *50*, 11947−11951.
(28) Mączka, M.; Gągor, A.; Macalik, B.; Pikul, A.; Ptak, M.; Hanuza, J. *Inorg.Chem.* **2014**, *53*, 457−467.
(29) Thomson, R. I.; Jain, P.; Cheetham, A. K.; Carpenter, M. A. *Phys. Rev. B* **2012**, *86*, 214304.
(30) Li, W.; Zhang, Z.; Bithell, E. G.; Batsanov, A. S.; Barton, P. T.; Saines, P. J.; Jain, P.; Howard, C. J.; Carpenter, M. A.; Cheetham, A. K. *Acta Mater.* **2013**, *61*, 4928−4938.
(31) Baker, P. J.; Lancaster, T.; Franke, I.; Hayes, W.; Blundell, S. J.; Pratt, F. L.; Jain, P.; Wang, Z.-M.; Kurmoo, M. *Phys. Rev. B* **2010**, *280*, 18−21.
(32) Tian, Y.; Wang, W.; Chai, Y.; Cong, J.; Shen, S.; Yan, L.; Wang, S.; Han, X.; Sun, Y. *Phys. Rev. Lett.* **2014**, *112*, 017202.
(33) Xu, G.-C.; Zhang, W.; Ma, X.-M.; Chen, Y.-H.; Zhang, L.; Cai, H.-L.; Wang, Z.-M.; Xiong, R.-G.; Gao, S. *J. Am. Chem. Soc.* **2011**, *133*, 14948−14951.
(34) Wang, Z.; Zhang, B.; Inoue, K.; Fujiwara, H.; Otsuka, T.; Kobayashi, H.; Kurmoo, M. *Inorg. Chem.* **2007**, *46*, 437−445.
(35) Xu, G.-C.; Ma, X.-M.; Zhang, L.; Wang, Z.-M.; Gao, S. *J. Am. Chem. Soc.* **2010**, *132*, 9588−9590.
(36) Mączka, M.; Pietraszko, A.; Macalik, B.; Hermanowicz, K. *Inorg. Chem.* **2014**, *53*, 787−794.
(37) Shannon, B. Y. R. D.; H, M.; Baur, N. H.; Gibbs, O. H.; Eu, M.; Cu, V. *Acta Crystallogr., Sect. A* **1976**, *32*, 751−767.
(38) Antsyshkina, A. S.; Porai-Koshits, M. A.; Ostrikova, V. N.; Sadikov, G. G. *Sov. J. Coord. Chem.* **1983**, *9*, 855−858.
(39) Sheldrick, G. M. *SHELXS-97: Program for Crystal Structure Resolution*; University of Göttingen: Göttingen, Germany, 1997.
(40) Sheldrick, G. M. *SHELXL-97: Program for Crystal Structure Analysis*; University of Göttingen: Göttingen, Germany, 1997.
(41) Howard, C. J.; Hunter, B. A. *Rietica: A Computer Program for Rietveld Analysis of X-ray and Neutron Powder Diffraction Patterns*; Australian Nuclear Science and Technology Organization Lucas Heights Research Laboratories: Menai, N.S.W., Australia, 1998.
(42) Boehler, R. *Rev. Sci. Instrum.* **2006**, *77*, 115103.
(43) Kresse, G.; Furthmüller, J. *Phys. Rev. B: Condens. Matter Mater. Phys.* **1996**, *54*, 11169−11186.
(44) Perdew, J.; Burke, K.; Ernzerhof, M. *Phys. Rev. Lett.* **1996**, *77*, 3865−3868.
(45) King-Smith, R. D.; Vanderbilt, D. *Phys. Rev. B* **1993**, *47*, 1651−1654.
(46) Le Bail, A.; Duroy, H.; Fourquet, J. L. *Mater. Res. Bull.* **1988**, *23*, 447−452.
(47) Duan, Z.; Wang, Z.; Gao, S. *Dalton Trans.* **2011**, *40*, 4465−4473.
(48) Eikeland, E.; Lock, N.; Filsø, M.; Stingaciu, M.; Shen, Y.; Overgaard, J.; Iversen, B. B. *Inorg. Chem.* **2014**, *53*, 10178−10188.
(49) Paredes-García, V.; Vega, A.; Novak, M. A.; Vaz, M. G. F.; Souza, D. A.; Venegas-Yazigi, D.; Spodine, E. *Inorg. Chem.* **2009**, *48*, 4737−4742.
(50) Kieslich, G.; Sun, S.; Cheetham, A. K. *Chem. Sci.* **2014**, *5*, 4712−4715.
(51) Orobengoa, D.; Capillas, C.; Aroyo, M. I.; Perez-Mato, J. M. *J. Appl. Crystallogr.* **2009**, *42*, 820−833.
(52) Kroumova, E.; Aroyo, M. I.; Perez-Mato, J. M.; Ivantchev, S.; Igartua, J. M.; Wondratschek, H. *J. Appl. Crystallogr.* **2001**, *34*, 783−784.
(53) Li, W.; Probert, M. R.; Kosa, M.; Bennett, T. D.; Thirumurugan, A.; Burwood, R. P.; Parinello, M.; Howard, J. A. K.; Cheetham, A. K. *J. Am. Chem. Soc.* **2012**, *134*, 11940−11943.
(54) Sánchez-Andújar, M.; Gómez-Aguirre, L. C.; PatoDoldán, B.; Yáñez-Vilar, S.; Artiaga, R.; Llamas-Saiz, A. L.; Manna, R. S.; Schnelle, F.; Lang, M.; Ritter, F.; Haghighirad, A. A.; Señarís-Rodríguez, M. A. *CrystEngComm* **2014**, *16*, 3558−3566.
(55) Bohatý, L.; Bayarjargal, L.; Becker, P. *Appl. Phys. B: Laser Opt.* **2007**, *86*, 523−527.
(56) Deserno, U.; Haussuhl, S. *IEEE J. Quantum Electron.* **1973**, *9*, 598−601.
(57) Bechthold, P. S.; Haussühl, S. *Appl. Phys.* **1977**, *14*, 403−410.
(58) Bayarjargal, L.; Winkler, B. *Z. Kristallogr.* **2014**, *229*, 92−100.
(59) Bator, G.; Baran, J.; Jakubas, R.; Sobczyk, L. *J. Mol. Struct.* **1998**, *450*, 89−100.
(60) Hadrich, A.; Lautie, A.; Mhiri, T. *J. Raman Spectrosc.* **2000**, *31*, 587−593.
(61) Mączka, M.; Pietraszko, A.; Macalik, B.; Hermanowicz, K. *Inorg. Chem.* **2014**, *53*, 787−794.
(62) Mączka, M.; Kadłubański, P.; Freire, P. T. C.; Macalik, B.; Paraguassu, W.; Hermanowicz, K.; Hanuza, J. *Inorg. Chem.* **2014**, *53*, 9615−9624.

DOI: 10.1021/ic502218n
Inorg. Chem. 2015, 54, 2109−2116